

Intense boundary emission destroys normal radio-frequency plasma sheath

Guang-Yu Sun, An-Bang Sun, and Guan-Jun Zhang*

Research Center for Advanced High Voltage and Plasma Technology, State Key Laboratory of Electrical Insulation and Power Equipment, Xi'an Jiaotong University, Xi'an 710049, China

Current models of capacitively coupled plasma indicate that external bias is mainly consumed by oscillating sheathes which shield external field. We report first evidence that strong boundary emission destroys normal radio-frequency (RF) sheath and establishes a new RF plasma where external bias is consumed by bulk plasma instead of sheathes. This produces ion confinement and intense RF current in bulk plasma, combined with unique particle and energy balance. Proposed model offers new method for ion erosion mitigation, wave mode conversion and a reaction rate control technic in low pressure plasma processing.

A capacitively coupled plasma (CCP) is naturally formed by applying radio-frequency (RF) voltage to electrodes. Understanding RF plasma properties is of fundamental interests and is essential in numerous applications¹⁻⁷. Contemporary models of CCP discharge assume that the bulk plasma is well isolated from the boundaries by oscillating sheathes and applied bias mainly rests on sheathes instead of bulk plasma. Conduction current prevails displacement current in bulk plasma and field in bulk plasma is weak. But in this letter we will show that the bias can be primarily consumed by bulk plasma and electric field in plasma center needs not to be shielded by sheathes, due to intense boundary emission.

Numerous studies have been done regarding boundary emission in CCP, but its influences are mostly assumed to be unessential^{4,8-15}. The steady flux of ion Γ_i produces a surface emission flux $\Gamma_{em} = \gamma_i \Gamma_i$ due to ion-induced secondary electron emission (SEE), with γ_i the emission coefficient. Under low pressure, secondary electrons (SEs) are lost before remarkable ionizations occur and their impact is less significant than that of hot electrons generated by stochastic heating¹⁶. Higher pressure incurs transition to γ mode where particle balance is modified by ionizations of SEs¹⁰. Yet the structure of plasma, i.e. bulk plasma connected by Bohm presheath and Child-law sheath, is supposed to be untouched and mean wall potential remains negative relative to plasma¹⁷⁻²¹.

In this letter, we show that boundary emission can bring very strong disturbance and restructure entire RF plasma, which happens when Γ_{em} is greater than averaged plasma electron flux $\langle \Gamma_{ep} \rangle_T$. It is well known that a space-charge limited (SCL) sheath is formed if $\Gamma_{em} > \Gamma_{ep}$ near floating boundary, such as thermionic emitter, emissive probe, Hall thruster, etc²²⁻²⁴. In this case, normal Child-law sheath still presents between plasma and the potential dip called virtual cathode (VC) near boundary, so dynamics of plasma are not essentially modified²⁵. Recent works reported that a floating SCL sheath can become unstable due to cold ion trapping^{26,27}. But no one has studied a RF plasma with intense boundary emission. Below we shall first show with simulation how RF plasma properties behave

*Email address: gjzhang@xjtu.edu.cn

under boundary emission, a theoretical ground is then given to validate simulation results. Model generality, practical methods for implementation, prospects in future applications are discussed as well.

To investigate RF plasma with boundary emission, we employ a 1D1V kinetic simulation code which advances kinetic equation and solves Poisson equation in each step. RF plasma bounded by two parallel planar electrodes is considered. Sinusoidal source is fixed as Dirichlet-type condition at boundaries. Adopted simulation parameters are listed below to help replicate simulation results: source frequency 13.56 MHz, bulk plasma density $n_0 = 5 \times 10^{14} \text{ m}^{-3}$, plasma electron temperature $T_{ep} = 14 \text{ eV}$, emitted electron temperature $T_{em} = 2.5 \text{ eV}$, ion temperature $T_i = 0.05 \text{ eV}$, ion mass 1u. Simulation domain length $L = 0.1 \text{ m}$, space resolution $\Delta x = 10^{-4} \text{ m}$. Range of electron/ion velocity is $4v_{Tep} = 4\sqrt{\frac{Tep}{m_e}}$ and $2c_s = 2\sqrt{\frac{Tep}{m_i}}$, divided into 601 points. Time step $\Delta t = 2 \times 10^{-3} \text{ ns}$. The simulation produces noise-free data for better understanding of sheath physics, similar methods were used in several previous works related to plasma sheath²⁸⁻³¹. More detailed algorithm was shown in our previous works of bounded plasma^{15,32}.

When boundary emission prevails plasma electron flux, the normal flux balance in average, i.e. $\langle \Gamma_{ep} - \Gamma_i - \Gamma_{em} \rangle_T = 0$ no longer holds since ion flux should be nonnegative, indicating that classical CCP breaks down when $\Gamma_{em} \geq \Gamma_{ep}$. The structure of RF plasma under intense boundary emission is given by simulation in Fig. 1a where two tiny sheath barriers with positive potential relative to sheath edge present near the surfaces, and nearly entire applied bias is absorbed by bulk plasma. We note this new RF plasma *inverted* RF plasma (IRP) as its sheath potential is inverted. Note that IRP is fundamentally different from previously observed field reversal in CCP, as the latter is a local and transient effect so the global CCP properties remain unchanged^{33,34}.

Simulation shows that electric field in bulk plasma equals to $E_b = \frac{\tilde{V}}{a} \cos(\omega t)$ with d the half of gap distance and \tilde{V} half of applied gap voltage amplitude. In Fig. 1b total current of normal CCP leads that of inverted RF plasma by nearly $\frac{\pi}{2}$, the latter coincides with source voltage. This phenomenon is highly unusual as oscillating sheath in CCP contains capacitance $C_{sh} = a \frac{\epsilon_0 A}{s_{sh}}$ with A the electrode area, s_{sh} sheath size and a a constant depending on model assumptions¹⁶. Normally the voltage across two capacitive sheathes V_{sh} far exceeds plasma voltage V_p and current is $\frac{\pi}{2}$ ahead of voltage. Field is much stronger in sheath where strong displacement current J_d fulfills the continuity. Note that in bulk of CCP the conduction current J_c prevails as only weak field penetrates therein.

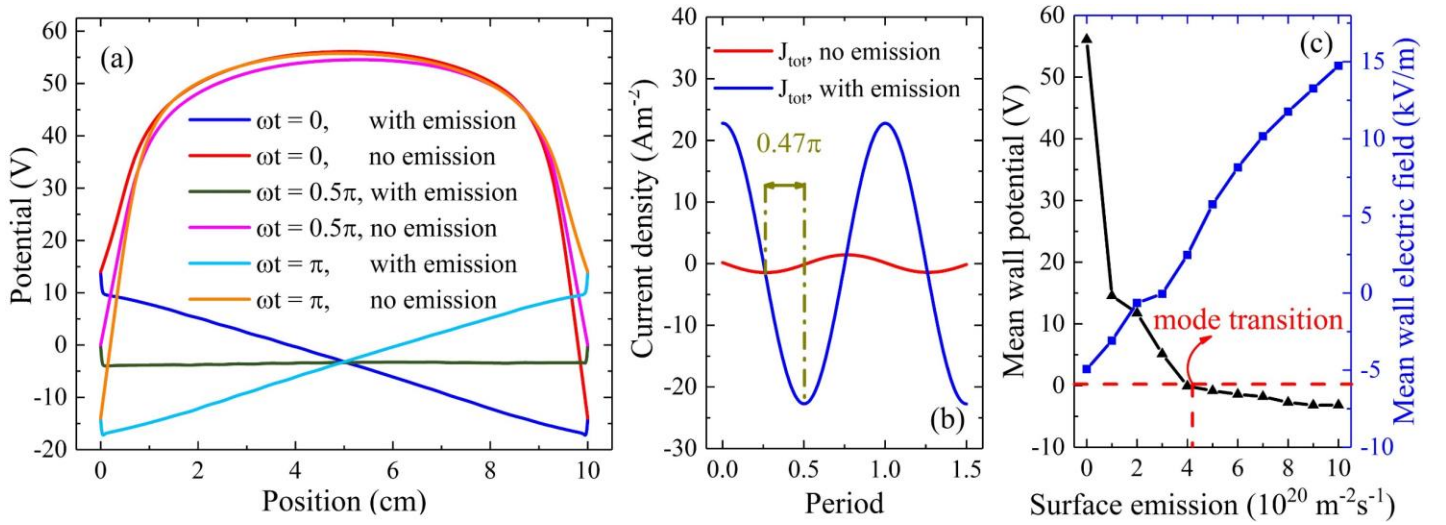


Figure 1. Simulation results of RF plasma with/without boundary emission. In (a) potentials of normal CCP are compared to condition with surface emission of $10^{21} \text{ m}^2 \text{ s}^{-1}$, which is around twice the initial plasma electron flux. Applied bias is consumed by bulk plasma and two small sheaths opposite to normal RF sheaths appear at both ends. In (b) the total currents of same conditions in (a) are compared. They have a phase difference of nearly 0.5π and boundary emission enlarges total current by more than 1 order of magnitude. External source is $\bar{V} \cos(\omega t)$. Panel (c) shows the transition from normal case to the new RF plasma by increasing Γ_{em} . Signs of sheath potential and field are inverted after $\Gamma_{em} \geq \Gamma_{ep}$.

The reason that an IRP behaves as above can be understood considering flux of plasma electrons. Fig. 1c shows that a mode transition from CCP to IRP occurs when Γ_{em} surpasses Γ_{ep} , combined by an inversion of wall potential and field. When wall potential is positive relative to sheath edge, plasma electron flux is unobstructed. Conduction current and displacement current in normal CCP and IRP are shown in Fig. 2a, b for comparison. Wall potential is negative relative to sheath edge in CCP, repelling most plasma electrons back hence the current continuity in sheath must be carried by displacement current. This is, however, unnecessary when wall potential is positive. Intense conduction current travels unimpeded in bulk plasma as well as sheath, calculated by $J_{c,IRP} = \sigma_p E_b = \frac{n_0 e^2 \bar{v}}{m_e \bar{v}_m d} \cos(\omega t) \approx 27.877 \cos(\omega t) \text{ A/m}^2$. Here σ_p is plasma dielectric constant and \bar{v}_m is collision frequency. Amplitude given by simulation is 23.02 A/m^2 , which is not far from estimation.

Flux balance in IRP becomes clear with above analyses. Fig. 2c, d give the distribution functions in two types of RF plasma. Ions respond to mean potential ($\omega \ll \omega_{pe}$) where no Bohm presheath presents and mean sheath potential is positive, hence Γ_i is confined while Γ_{ep} conserves. Emitted electron from boundary are partially reflected back to surface by inverted sheath barrier and some penetrate into plasma. The flux balance is therefore written as $\langle \Gamma_{ep} + \Gamma_{eref} - \Gamma_{em} \rangle_T = 0$ with Γ_{eref} the flux of reflected emitted electrons towards boundary. Γ_{em} is constant in simulation, possibly representing thermionic emission or photoemission, but can also be a function of Γ_{ep} due to SEE³⁵. The unique particle and power balance in IRP will be analyzed following a theoretical ground to be established below.

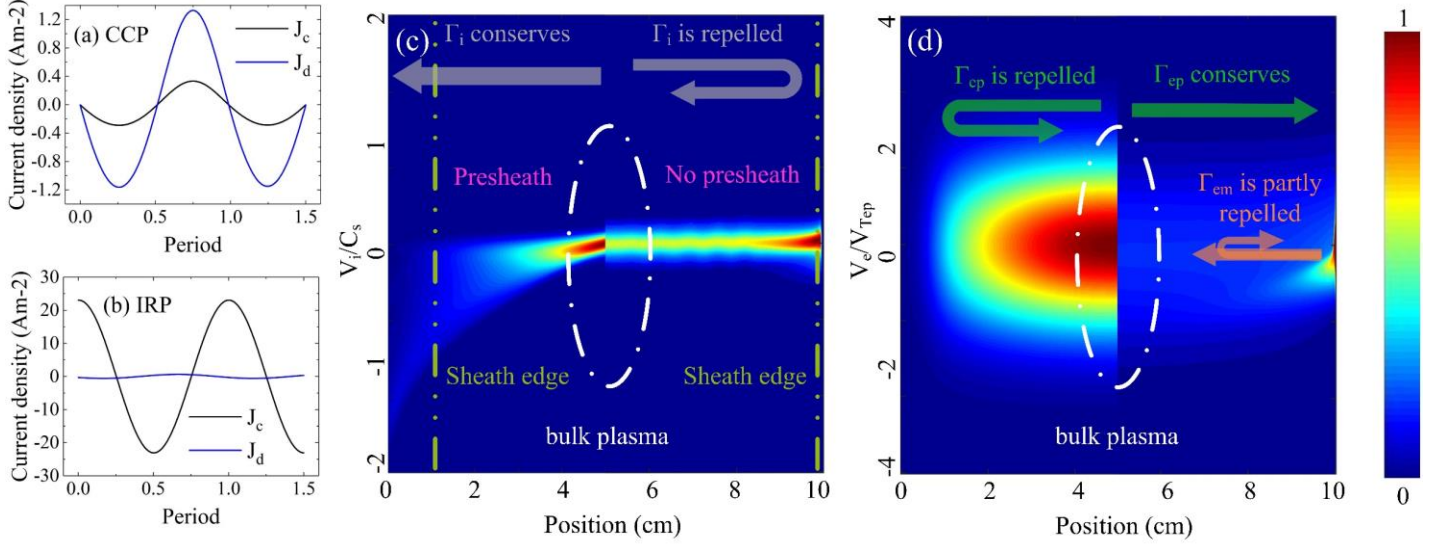


Figure 2. (a), (b) show J_c and J_d in sheath of CCP and IRP. $J_d \gg J_c$ in CCRF sheath while $J_c \gg J_d$ in inverted RF sheath. (c)(d) give normalized ion and electron velocity distribution functions (VDFs) when $\omega t = 0.5\pi$ for CCP (left panel) and IRP (right panel). In CCP electrons are repelled and ion flux conserves. In IRP plasma electrons are unobstructed and ions are confined. Velocity space is normalized to $v_{Tep} = \sqrt{\frac{T_{ep}}{m_e}}$ and $c_s = \sqrt{\frac{T_{ep}}{m_i}}$.

Typical model in normal CCP is based on step function model, assuming a time-dependent sheath edge out of which electron density equals to zero. A Child-law type sheath and Bohm presheath are chosen as prerequisite^{18,19,36,37}. However, they are no longer valid for IRP and new theoretical ground should be established. Below we will first deduce inverted sheath potential and then solve the whole IRP. Two key parameters are defined as follows: (1) mean inverted sheath $\overline{\varphi_{inv}}$ representing mean potential of plasma center relative to wall; (2) temporal inverted sheath $\varphi_{inv}(\omega t)$ representing real-time wall potential relative to sheath edge. The former characterizes ion dynamics and the latter is for electrons. Both parameters are chosen as positive for simplicity.

Enforcing boundary condition $V_{wall} = \tilde{V}\cos(\omega t)$, the following equation is derived:

$$-\overline{\varphi_{inv}} + E_{tran}(\omega t)x_s(\omega t) + \varphi_{inv}(\omega t) = \tilde{V}\cos(\omega t) \quad (1)$$

with x_s the location of sheath edge. If the total length between plasma center and wall is d , a simplified expression of temporal inverse sheath barrier is obtained:

$$\varphi_{inv}(\omega t) = \frac{\beta en_0}{2\epsilon_0} [d - x_s(\omega t)]^2 \quad (2)$$

where β is an adjustable parameter generally equal or greater than 1, representing electron density in inverted RF sheath. Ions are assumed to be cold.

Using basic plasma kinetic theories, electron density in temporal inverse sheath are derived as follows:

$$n_{ep}(\varphi) = n_{ep0} \exp\left(\frac{e\varphi}{T_{ep}}\right) \operatorname{erfc}\left(\sqrt{\frac{e\varphi}{T_{ep}}}\right) \quad (3a)$$

$$n_{em}(\varphi) = n_{emw} \exp\left[\frac{e(\varphi - \varphi_{inv}(\omega t))}{T_{em}}\right] \quad (3b)$$

$$n_{eref}(\varphi) = n_{em}(\varphi) \operatorname{erf}\left(\sqrt{\frac{e\varphi}{T_{em}}}\right) \quad (3c)$$

Here n_{ep0} is plasma electron density at sheath edge and n_{emw} is emitted electron density at wall, deductions of Eq. 4 are based on integration of EVDF which can be commonly found in many related works of sheath physics^{23,38-40}. Taking both emitted electron and plasma electron flux as half-Maxwellian, we obtain $\Gamma_{ep} = n_{ep0} \sqrt{\frac{2T_{ep}}{\pi m_e}}$, $\Gamma_{em} = n_{emw} \sqrt{\frac{2T_{em}}{\pi m_e}}$. Reflected electron flux and penetrating flux marked out in Fig. 2d are $\Gamma_{eref} = \Gamma_{em} [1 - \exp(-\frac{e\varphi_{inv}(\omega t)}{T_{em}})]$ and $\Gamma_{epen} = \Gamma_{em} \exp(-\frac{e\varphi_{inv}(\omega t)}{T_{em}})$, respectively.

In addition, the charge neutrality at sheath edge must hold, which gives $n_{ep}(\varphi) + n_{em}(\varphi) + n_{eref}(\varphi)|_{sheath\ edge} = n_0$. the following relation is obtained:

$$\varphi_{inv}(\omega t) = \frac{(M + \sqrt{M^2 + 4\overline{\varphi_{inv}}})^2}{4} \quad (4)$$

with $M = \sqrt{\frac{2\varepsilon_0}{\beta en_0 d}} \tilde{V} \cos(\omega t)$. It is then possible to calculate both $\varphi_{inv}(\omega t)$ and $\overline{\varphi_{inv}}$ with abovementioned flux balance in average

$\frac{1}{2\pi} \int_0^{2\pi} (\Gamma_{ep} + \Gamma_{eref} - \Gamma_{em}) d(\omega t) = 0$. Validity of above deductions can be briefly justified with two limits below:

$$\overline{\varphi_{inv}}|_{\tilde{V}=0} = \varphi_{inv}(\omega t)|_{\tilde{V}=0} = \frac{T_{em}}{e} \ln\left(\frac{\Gamma_{em}}{\Gamma_{ep}}\right) \quad (5a)$$

$$\varphi_{inv}(\omega t)|_{\tilde{V} \rightarrow +\infty} = \begin{cases} M^2, \omega t \in [k\pi, (k+0.5)\pi], k \in \mathbb{Z}^{\geq} \\ 0, \omega t \notin [k\pi, (k+0.5)\pi], k \in \mathbb{Z}^{\geq} \end{cases} \quad (5b)$$

Limits in Eq. 5 show that the RF sheath is reduced to floating inverse sheath when $\tilde{V} = 0$. Temporal inverted sheath is rectified in half period when $\tilde{V} \rightarrow +\infty$. Once $\overline{\varphi_{inv}}$ and $\varphi_{inv}(\omega t)$ are determined, potential in entire IRP can be calculated by solving Poisson's equation, which requires an order reduction with the numerical integral below:

$$\left(\frac{d\varphi}{dx}\right)^2 \Big|_0^\varphi = \frac{2n_{ep0}T_{ep}}{\varepsilon_0} \left[\exp\left(\frac{e\varphi}{T_{ep}}\right) - 1 - \mathcal{F}(\varphi, T_{ep}) \right] + \frac{2n_{emw}T_{em}}{\varepsilon_0} \exp\left(-\frac{e\varphi_{inv}(\omega t)}{T_{em}}\right) \left[\exp\left(\frac{e\varphi}{T_{em}}\right) - 1 + \mathcal{F}(\varphi, T_{em}) \right] \quad (6)$$

where n_{emw} is given by Γ_{em} , n_{ep0} is solved from charge neutrality and $\mathcal{F}(\varphi, T) = \exp\left(\frac{e\varphi}{T}\right) \operatorname{erf}\left(\sqrt{\frac{e\varphi}{T}}\right) - 2\sqrt{\frac{e\varphi}{\pi T}}$. Calculated potentials

are given in Fig. 3a, showing good agreement with simulation. Calculated $\overline{\varphi_{inv}}$ is somewhat higher due to assumption of cold ions

and collisionless sheath. Fig. 3b shows $\varphi_{inv}(\omega t)$ with different source voltages. They are normalized by $\overline{\varphi_{inv}}$ to facilitate comparison. For small \tilde{V} it is collinear with sinusoidal source but it gradually approaches the limit of Eq. 5b and becomes rectified at half period when \tilde{V} is large. A complete rectification occurs when $\tilde{V} \rightarrow +\infty$, yet higher ionization rate may alter the realistic condition from the ideal limit. Calculated $\overline{\varphi_{inv}}$ is shown in Fig. 3c. The mean sheath barrier rises up with both Γ_{em} and \tilde{V} , making it possible to control the ion confinement by changing boundary emission and source amplitude. Note the emission threshold above which IRP is formed increases with \tilde{V} .

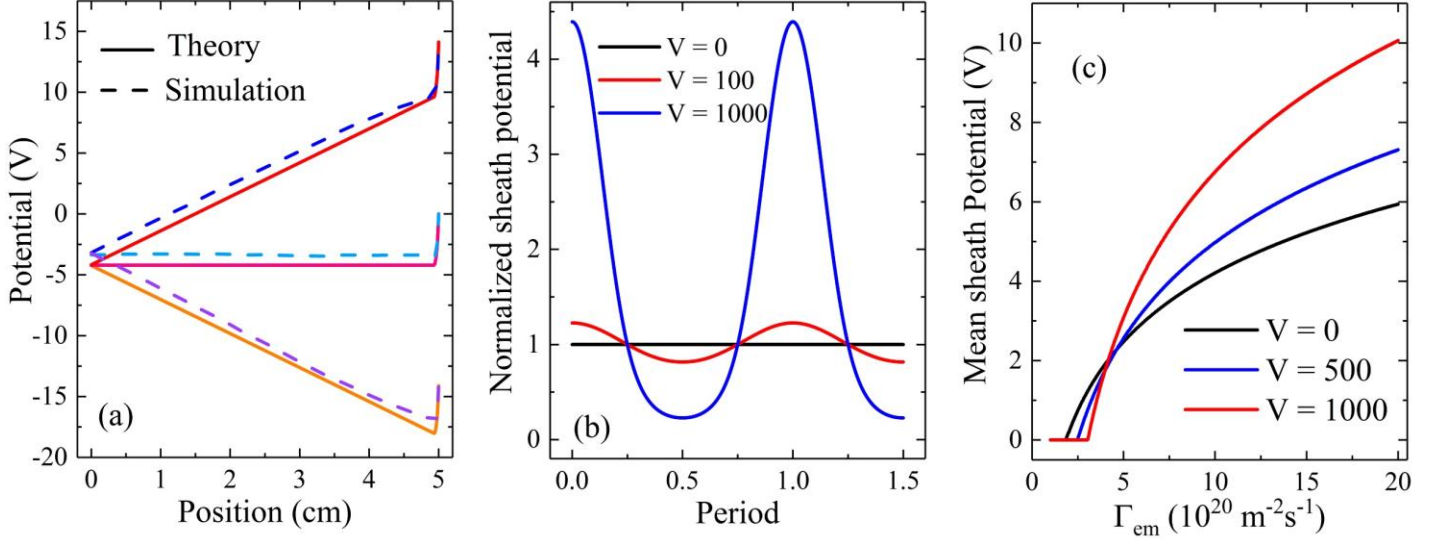


Figure 3. Results from theory. In (a) the same parameters as in simulation are used to calculate space potential in IRP at $\omega t = 0, 0.5\pi, \pi$. (b) gives $\frac{\varphi_{inv}(\omega t)}{\overline{\varphi_{inv}}}$ at different \tilde{V} , unit V. $\tilde{V} = 0$ gives floating inverse sheath (Eq. 5a), sheath potential is sinusoidal for small \tilde{V} , for large \tilde{V} it is rectified in half period (Eq. 5b). (c) shows $\overline{\varphi_{inv}}$ with different Γ_{em} and \tilde{V} . The minimum \tilde{V} to invoke IRP increases with \tilde{V} , and $\overline{\varphi_{inv}}$ increases with Γ_{em} .

The dominant bias consumption by bulk plasma and non-shielding field lead to unique particle and power balance, which can be derived based on above analyses. For particle balance, ionizations should compensate for ion loss at boundaries. Ion flux is conserved in CCP while in IRP only energetic ions crossing $\overline{\varphi_{inv}}$ can hit the wall, which requires lower ionization rate. The electron power balance in CCP is written as $S_{coll} + S_{edge} = S_{ohm} + 2S_{stoc}$ ⁸, indicating that power gained from ohmic heating and stochastic heating is equal to power lost due to collisions and boundary flux. The LHS is frequently written as $2\Gamma_e e(\mathcal{E}_c + \mathcal{E}_{e,loss})$. The power balance should be modified in IRP. The mean energy of incident electrons at walls $\langle \mathcal{E}_e \rangle$ is $\frac{T_{ep}}{2}$ for 1D Maxwellian in CCP and is $\int_{\sqrt{\frac{2e\overline{\varphi_{inv}(\omega t)}}{m_e}}}^{\infty} f_{ep}(v, T_{ep}) \frac{m_e}{2} v^2 dv$ in IRP since they are accelerated. Ohmic heating is similar in both cases, but IRP contains higher ohmic heating as conduction current is intense. It is worthwhile to mention that the stochastic heating is zero in inverted RF plasma since presheath is flat. Stochastic heating in normal CCP discharge is due to non-synchronous motion of sheath edge and bulk plasma, which can be verified by current continuity $n_{e,sheath} v_{e,sheath} = n_{e,bulk} v_{e,bulk}$.⁴¹ The drop of plasma density in Bohm presheath makes

$v_{e,sheath} \neq v_{e,bulk}$ so a velocity modulation takes place, which cannot happen in inverted RF plasma where presheath is flat and plasma electron density is uniform. Deduced expressions between two types of RF plasma are given in Table I.

TABLE I. Particle balance, energy loss per plasma electron/ion hitting the wall, ohmic heating, stochastic heating in CCP and IRP. K_{iz} is ionization rate, n_g is gas density, $u_B = \sqrt{\frac{T_{ep}}{m_i}}$, $\langle \mathcal{E}_e \rangle$ and $\langle \mathcal{E}_i \rangle$ are mean incident energies of electron and ion at boundaries, V_s is sheath potential in CCP, d_b is length of bulk plasma, u_{sh} is velocity of oscillating sheath in CCP.

Type	$n_0 K_{iz} n_g d_b$	$\mathcal{E}_{e,loss}$	$\mathcal{E}_{i,loss}$	S_{ohm}	S_{stoc}
CCP	$2n_0 u_B$	$\frac{T_{ep}}{2} + eV_s + \langle \mathcal{E}_e \rangle$	$\frac{T_{ep}}{2} + eV_s$	$\frac{1}{2} J^2 \frac{d_b}{\sigma_p}$	$\sqrt{\frac{2m_e T_{ep}}{\pi}} n_0 u_{sh}^2$
IRP	$2n_0 \sqrt{\frac{2T_i}{\pi m_i}} \exp\left(-\frac{e\overline{\varphi_{inv}}}{T_i}\right)$	$\langle \mathcal{E}_e \rangle$	$\langle \mathcal{E}_i \rangle + e\overline{\varphi_{inv}}$	$\frac{1}{2} J^2 \frac{d_b}{\sigma_p}$	0

Above analyses show that IRP contains three unique features namely ion confinement, intense RF current and non-shielding RF field. To realize it in practice, one can capitalize on boundary emission though SEE^{32,42,43}, thermionic emission^{26,29,44} and photoemission⁴⁵⁻⁴⁷. In boundaries of many RF-heated plasma systems, ion flux is damaging, e.g. plasma thruster⁴⁸, tokamak edge region⁴⁹⁻⁵¹, etc. Ion flux induces wall erosion and impurity influx⁵², which can be eradicated by invoking IRP. The fact that $\overline{\varphi_{inv}}$ rises up with applied voltage makes it possible to confine hot ions with limited boundary emission, consider the fact that generating very intense Γ_{em} may be difficult in practice.

Another promising prospect of IRP is plasma-based material processing. Ion flux is not easy to control in collisionless sheath since it conserves. Invoking IRP can monitor ion flux as well as ion incident energy, according to $\Gamma_{i,wall} = \Gamma_{i0} \exp\left(-\frac{e\overline{\varphi_{inv}}}{T_i}\right)$ and Tab I, with $\overline{\varphi_{inv}}$ adjustable with respect to Γ_{em} and \tilde{V} . The maximum ion flux Γ_{i0} is instantly available by switching IRP off, offering possibility to control reaction rate in etching, deposition, synthesis, etc^{16,34,53}.

Also, the large RF current in IRP can generate electrostatic waves which may be further converted into electromagnetic waves. Electrostatic waves can be excited by applying RF voltage on matched probe immersed in plasma, to be detected and amplified for measurement^{54,55}. Strong electrostatic waves generated in IRP can be transformed to electromagnetic radiation through mode conversion in inhomogeneous plasma^{56,57}, which is expected to be implemented in related experiments. Note that transverse field shielding is not exactly the same as the model proposed here. It remains unknown for the moment whether IRP can be formed in inductively coupled plasma (ICP). A recent experiment reported a positive potential of highly emissive probe relative to plasma in ICP, though the complete sheath profile was unknown³⁵. Yet most others reported negative potential relative to plasma⁵⁸⁻⁶¹. Future

works are encouraged for IRP with transverse waves, which offers possibilities to overcome blockage of signal by plasma layer in spacecraft communications⁶².

In conclusion, we show with simulation and theory that boundary emission in RF plasma can produce strong disturbance and establishes a new inverted RF plasma different from normal CCP. Applied bias is mainly consumed by bulk plasma instead of sheath, also field is not shielded by sheath. It naturally confines ions and shows nonclassical sheath coupling, presheath-sheath structure, particle and energy balance, etc. Invoking inverted RF plasma mitigates wall erosion and impurity flux in plasma thruster, tokamak edge region where excessive ion flux is damaging. It also provides inspiration for new reaction control technic in plasma processing.

Acknowledgements

Guang-Yu Sun would like to thank Dr. M.D. Campanell in Lawrence Livermore National Laboratory for his help in modeling and Dr. I. D. Kaganovich, A.V. Khrabrov in Princeton Plasma Physics Laboratory for fruitful discussions. Authors also thank Prof. Ute Ebert at CWI Amsterdam and Dr. Markus Becker at INP Greifswald for their kind suggestions. This research was conducted under the auspices of National Natural Science Foundation of China (NSFC) under Grant No. 51827809, U1766218.

References

- 1 Bruneau, B., Gans, T., O'Connell, D., Greb, A., Johnson, E. V. & Booth, J.-P. Strong Ionization Asymmetry in a Geometrically Symmetric Radio Frequency Capacitively Coupled Plasma Induced by Sawtooth Voltage Waveforms. *Physical Review Letters* **114**, 125002 (2015).
- 2 Turner, M. M. & Chabert, P. Collisionless Heating in Capacitive Discharges Enhanced by Dual-Frequency Excitation. *Physical Review Letters* **96**, 205001 (2006).
- 3 Kaganovich, I. D. Anomalous Capacitive Sheath with Deep Radio-Frequency Electric-Field Penetration. *Physical Review Letters* **89**, 265006 (2002).
- 4 Zhao, K., Wen, D.-Q., Liu, Y.-X., Lieberman, M. A., Economou, D. J. & Wang, Y.-N. Observation of Nonlinear Standing Waves Excited by Plasma-Series-Resonance-Enhanced Harmonics in Capacitive Discharges. *Physical Review Letters* **122**, 185002 (2019).
- 5 Boeuf, J.-P. & Chaudhury, B. Rotating Instability in Low-Temperature Magnetized Plasmas. *Physical Review Letters* **111**, 155005 (2013).
- 6 Liu, Y.-X., Schüngel, E., Korolov, I., Donkó, Z., Wang, Y.-N. & Schulze, J. Experimental Observation and Computational Analysis of Striations in Electronegative Capacitively Coupled Radio-Frequency Plasmas. *Physical Review Letters* **116**, 255002 (2016).
- 7 Schulze, J., Derzsi, A., Dittmann, K., Hemke, T., Meichsner, J. & Donkó, Z. Ionization by Drift and Ambipolar Electric Fields in Electronegative Capacitive Radio Frequency Plasmas. *Physical Review Letters* **107**, 275001 (2011).

- 8 Misium, G. R., Lichtenberg, A. J. & Lieberman, M. A. Macroscopic modeling of radio - frequency
plasma discharges. *Journal of Vacuum Science & Technology A* **7**, 1007-1013 (1989).
- 9 Lafleur, T., Chabert, P. & Booth, J. P. Secondary electron induced asymmetry in capacitively coupled
plasmas. *Journal of Physics D: Applied Physics* **46**, 135201 (2013).
- 10 Sun, A., Becker, M. M. & Loffhagen, D. PIC/MCC simulation of capacitively coupled discharges in
helium: boundary effects. *Plasma Sources Science and Technology* **27**, 054002 (2018).
- 11 Liu, G.-H., Wang, X.-Y., Liu, Y.-X., Sun, J.-Y. & Wang, Y.-N. Effects of secondary electron emission
on plasma density and electron excitation dynamics in dual-frequency asymmetric capacitively coupled
argon plasmas. *Plasma Sources Science and Technology* **27**, 064004 (2018).
- 12 Orlov, K. E., Malik, D. A., Chernoziumskaya, T. V. & Smirnov, A. S. rf Electrode Sheath Formation
near a Concave Electrode. *Physical Review Letters* **92**, 055001 (2004).
- 13 Horváth, B., Daksha, M., Korolov, I., Derzsi, A. & Schulze, J. The role of electron induced secondary
electron emission from SiO₂ surfaces in capacitively coupled radio frequency plasmas operated at low
pressures. *Plasma Sources Science and Technology* **26**, 124001 (2017).
- 14 Liu, Q., Liu, Y., Samir, T. & Ma, Z. Numerical study of effect of secondary electron emission on
discharge characteristics in low pressure capacitive RF argon discharge. *Physics of Plasmas* **21**, 083511
(2014).
- 15 Sun, G.-Y., Li, H.-W., Sun, A.-B., Li, Y., Song, B.-P., Mu, H.-B., Li, X.-R. & Zhang, G.-J. On the role
of secondary electron emission in capacitively coupled radio-frequency plasma sheath: A theoretical
ground. *Plasma Processes and Polymers* **0**, e1900093 (2019).
- 16 Lieberman, M. A. & Lichtenberg, A. J. Principles of Plasma Discharges and Materials Processing
(2005).
- 17 Lafleur, T., Chabert, P. & Booth, J. P. Electron heating in capacitively coupled plasmas revisited. *Plasma
Sources Science and Technology* **23**, 035010 (2014).
- 18 Kaganovich, I. D., Polomarov, O. V. & Theodosiou, C. E. Revisiting the anomalous RF field penetration
into a warm plasma. *IEEE Transactions on Plasma Science* **34**, 696-717 (2006).
- 19 Kawamura, E., Lieberman, M. A. & Lichtenberg, A. J. Electron heating in low pressure capacitive
discharges revisited. *Physics of Plasmas* **21**, 123505 (2014).
- 20 Chabert, P. & Braithwaite, N. *Physics of Radio-Frequency Plasmas*. (Cambridge University Press,
2011).
- 21 Turner, M. M. Collisionless heating in radio-frequency discharges: a review. *Journal of Physics D:
Applied Physics* **42**, 194008 (2009).
- 22 Sydorenko, D., Kaganovich, I., Raitsev, Y. & Smolyakov, A. Breakdown of a Space Charge Limited
Regime of a Sheath in a Weakly Collisional Plasma Bounded by Walls with Secondary Electron
Emission. *Physical Review Letters* **103**, 145004 (2009).
- 23 Sheehan, J. P., Hershkowitz, N., Kaganovich, I. D., Wang, H., Raitsev, Y., Barnat, E. V., Weatherford,
B. R. & Sydorenko, D. Kinetic Theory of Plasma Sheaths Surrounding Electron-Emitting Surfaces.
Physical Review Letters **111**, 075002 (2013).
- 24 Autricque, A., Khrapak, S. A., Couëdel, L., Fedorczak, N., Arnas, C., Layet, J. M. & Grisolia, C.
Electron collection and thermionic emission from a spherical dust grain in the space-charge limited
regime. *Physics of Plasmas* **25**, 063701 (2018).
- 25 Hobbs, G. D. & Wesson, J. A. Heat flow through a Langmuir sheath in the presence of electron emission.
Plasma Physics **9**, 85-87 (1967).
- 26 Campanell, M. D. Alternative model of space-charge-limited thermionic current flow through a plasma.
Physical Review E **97**, 043207 (2018).
- 27 Campanell, M. D., Khrabrov, A. V. & Kaganovich, I. D. Absence of Debye Sheaths due to Secondary
Electron Emission. *Physical Review Letters* **108**, 255001 (2012).

- 28 Cagas, P., Hakim, A., Juno, J. & Srinivasan, B. Continuum kinetic and multi-fluid simulations of
classical sheaths. *Physics of Plasmas* **24**, 022118 (2017).
- 29 Campanell, M. D. & Johnson, G. R. Thermionic Cooling of the Target Plasma to a Sub-eV Temperature.
Physical Review Letters **122**, 015003 (2019).
- 30 Coulette, D. & Manfredi, G. An Eulerian Vlasov code for plasma-wall interactions. *Journal of Physics:
Conference Series* **561**, 012005 (2014).
- 31 Juno, J., Hakim, A., TenBarge, J., Shi, E. & Dorland, W. Discontinuous Galerkin algorithms for fully
kinetic plasmas. *Journal of Computational Physics* **353**, 110-147 (2018).
- 32 Sun, G.-Y., Li, Y., Zhang, S., Song, B.-P., Mu, H.-B., Guo, B.-H., Sun, A.-B. & Zhang, G.-J. Integrated
modeling of plasma-dielectric interaction: kinetic boundary effects. *Plasma Sources Science and
Technology* **28**, 055001 (2019).
- 33 Schulze, J., Donkó, Z., Heil, B. G., Luggenhölscher, D., Mussenbrock, T., Brinkmann, R. P. &
Czarnetzki, U. Electric field reversals in the sheath region of capacitively coupled radio frequency
discharges at different pressures. *Journal of Physics D: Applied Physics* **41**, 105214 (2008).
- 34 Krüger, F., Wilczek, S., Mussenbrock, T. & Schulze, J. Voltage waveform tailoring in radio frequency
plasmas for surface charge neutralization inside etch trenches. *Plasma Sources Science and Technology*
28, 075017 (2019).
- 35 Kraus, B. F. & Raitses, Y. Floating potential of emitting surfaces in plasmas with respect to the space
potential. *Physics of Plasmas* **25**, 030701 (2018).
- 36 Lieberman, M. A. Analytical solution for capacitive RF sheath. *IEEE Transactions on Plasma Science*
16, 638-644 (1988).
- 37 Mussenbrock, T., Brinkmann, R. P., Lieberman, M. A., Lichtenberg, A. J. & Kawamura, E.
Enhancement of Ohmic and Stochastic Heating by Resonance Effects in Capacitive Radio Frequency
Discharges: A Theoretical Approach. *Physical Review Letters* **101**, 085004 (2008).
- 38 Ordonez, C. A. Fully kinetic plasma - sheath theory for a cold - electron emitting surface. *Physics of
Fluids B: Plasma Physics* **4**, 778-783 (1992).
- 39 Schwager, L. A. & Birdsall, C. K. Collector and source sheaths of a finite ion temperature plasma.
Physics of Fluids B: Plasma Physics **2**, 1057-1068 (1990).
- 40 Campanell, M. D. Negative plasma potential relative to electron-emitting surfaces. *Physical Review E*
88, 033103 (2013).
- 41 Kawamura, E., Lieberman, M. A. & Lichtenberg, A. J. Stochastic heating in single and dual frequency
capacitive discharges. *Physics of Plasmas* **13**, 053506 (2006).
- 42 Wang, X., Pilewskie, J., Hsu, H. W. & Horányi, M. Plasma potential in the sheaths of electron-emitting
surfaces in space. *Geophysical Research Letters* **43**, 525-531 (2016).
- 43 Qing, S. & Zhao, Y. A detailed study on the structures of steady-state collisionless kinetic sheath near a
dielectric wall with secondary electron emission. II. Inverse and space-charge limited sheaths. *Physics
of Plasmas* **25**, 063520 (2018).
- 44 Campanell, M. D. & Umansky, M. V. Improved understanding of the hot cathode current modes and
mode transitions. *Plasma Sources Science and Technology* **26**, 124002 (2017).
- 45 Changmai, S. & Bora, M. P. Photoemission driven electron two-stream instability (ETSI) and evolution
of plasma sheath. *Physics of Plasmas* **26**, 042113 (2019).
- 46 Farrell, W. M., Poppe, A. R., Zimmerman, M. I., Halekas, J. S., Delory, G. T. & Killen, R. M. The lunar
photoelectron sheath: A change in trapping efficiency during a solar storm. *Journal of Geophysical
Research: Planets* **118**, 1114-1122 (2013).
- 47 Collier, M. R., Newheart, A., Poppe, A. R., Hills, H. K. & Farrell, W. M. Stair-step particle flux spectra
on the lunar surface: Evidence for nonmonotonic potentials? *Geophysical Research Letters* **44**, 79-87
(2017).

- 48 Bering, E. A., Chang-Diaz, F. & Squire, J. The use of rf waves in space propulsion systems. *URSI Radio Science Bulletin* **2004**, 92-106 (2004).
- 49 Kohno, H., Myra, J. R. & D'Ippolito, D. A. Numerical investigation of fast-wave propagation and radio-frequency sheath interaction with a shaped tokamak wall. *Physics of Plasmas* **22**, 072504 (2015).
- 50 Angelini, B. *et al.* Overview of the FTU results. *Nuclear Fusion* **45**, S227-S238 (2005).
- 51 Cardinali, A., Castaldo, C., Cesario, R., Marco, F. D. & Paoletti, F. Analysis of the heating scenarios of the ion Bernstein wave (IBW) experiment in Frascati Tokamak Upgrade. *Nuclear Fusion* **42**, 427-440 (2002).
- 52 Kumar, S. T. A., Den Hartog, D. J., Caspary, K. J., Magee, R. M., Mirnov, V. V., Chapman, B. E., Craig, D., Fiksel, G. & Sarff, J. S. Classical Impurity Ion Confinement in a Toroidal Magnetized Fusion Plasma. *Physical Review Letters* **108**, 125006 (2012).
- 53 Yatom, S., Selinsky, R. S., Koel, B. E. & Raitsev, Y. "Synthesis-on" and "synthesis-off" modes of carbon arc operation during synthesis of carbon nanotubes. *Carbon* **125**, 336-343 (2017).
- 54 Franklin, R. N., Hamberger, S. M., Lampis, G., Smith, G. J. & Holder, D. W. Nonlinear behaviour of a finite amplitude electron plasma wave I. Electron trapping effects. *Proceedings of the Royal Society of London. A. Mathematical and Physical Sciences* **347**, 1-24 (1975).
- 55 Franklin, R. N. & Braithwaite, N. S. J. Electron plasma waves and plasma resonances. *Plasma Sources Science and Technology* **18**, 014019 (2008).
- 56 Hinkel-Lipsker, D. E., Fried, B. D. & Morales, G. J. Conversion of electrostatic and electromagnetic waves in a plasma at the peak of a parabolic density profile. *Physical Review Letters* **66**, 1862-1865 (1991).
- 57 Kalae, M. J. & Katoh, Y. Study of a condition for the mode conversion from purely perpendicular electrostatic waves to electromagnetic waves. *Physics of Plasmas* **23**, 072119 (2016).
- 58 Ionita, C. *et al.* Plasma potential probes for hot plasmas. *The European Physical Journal D* **73**, 73 (2019).
- 59 Gyergyek, T. & Kovačič, J. Potential Formation in a Bounded Plasma System which is Terminated by an Electron Emitting Floating Collector Studied by a Particle-in-Cell Computer Simulation. *Contributions to Plasma Physics* **53**, 189-201 (2013).
- 60 Fruchtman, A., Zoler, D. & Makrinich, G. Potential of an emissive cylindrical probe in plasma. *Physical Review E* **84**, 025402 (2011).
- 61 Chen, X. & Sanchez-Arriaga, G. Orbital motion theory and operational regimes for cylindrical emissive probes. *Physics of Plasmas* **24**, 023504 (2017).
- 62 Bachynski, M. P. Electromagnetic wave penetration of reentry plasma sheaths. *RADIO SCIENCE Journal of Research* **2** (1965).